60. MRI Gradient Coil Optimization

F. David Doty

Doty Scientific, Inc. 700 Clemson Road, Columbia, SC 29229, USA

Abstract

A more complete set of largely dimensionless optimization parameters is introduced to better address the requirements of microscopy gradients. New parameters include DC efficiency, acoustic efficiency, nearest gradient null point, switching efficiency, continuous gradient rating, nerve stimulation, and volume current density ratios. The standard parameters of gradient uniformity, shielding effectiveness, recovery time, impedance matching, gradient gain, inductance, and rf shielding are also discussed. A novel design for transverse gradient coils utilizing crescent-shaped coils in combination with golay coils is shown to have substantial advantages in reduced acoustic response, increased continuous gradients, and reduced image fold back. Very high amplifier output impedance in constant current mode is also shown to be critical in certain applications.

60.1 Introduction

More than a decade after high-performance shielded gradients were introduced [1,2], there is still considerable confusion about the importance of various technical issues and performance parameters in gradient coil design. Some will insist that linearity is the main issue, others inductance or resistance, others gradient gain, and still others shielding. In truth, none of these in itself is very meaningful, though all are important when put into proper relationship to other parameters. In practice, one of the most important characteristics is reliability, which is most closely related to minimum conductor cross-section, encapsulation quality, and coil-form stiffness in smaller systems, though in larger systems it may be more dependent on cooling. An increasingly important parameter appears to be continuous gradient strength. However, the main point of this paper is that gradient optimization is a multi-dimensional problem. The two-orders-of-magnitude increase in com-

This article is a reprint from Spatially Resolved Magnetic Resonance
Methods, Materials, Medicine, Biology, Rheology, Geology, Ecology, Hardware

Edited by P. Blumler, B. Blumich, R. Botto, E. Fukushima - Wiley-VCH 1998

putational power per unit cost during the past decade has decreased the value of analytical optimization of a few parameters, and the method of error minimization is also now inconsequential. The focus must be on system requirements, design tradeoffs, cost, and construction of the objective function in the optimization routine, as all gradient designs have been done numerically for at least the last six years. Moreover, this paper will address only transverse gradients in detail, as axial gradients have been well covered in the literature. In addition to the gradient coil, we will look briefly at critical amplifier issues.

From a design perspective, the MRI gradient coil is best evaluated in terms of the following (mostly dimensionless) parameters: switching efficiency, differential (or local) linearity, relative residual eddy current gradient, settling time, DC efficiency, cooling effectiveness, and acoustic efficiency. The gradient amplifier is best evaluated in terms of VA (peak power) per dollar, power bandwidth, settling time to 0.2%, low frequency noise (1 - 1000 Hz), DC drift, constant-current (CC) output impedance, total harmonic distortion at 1 kHz, and power efficiency at ~ 30% of peak current and voltage. Optimizing the gradient inductance or resistance for a given amplifier is not particularly critical.

60.2 Definitions, Specifications, and Coil Optimization

60.2.1 Switching Efficiency

Because the inductive time constant is L/R, it is often asserted that one of the first objectives in gradient coil design is to minimize inductance, but it is trivial to reduce inductance by more than an order of magnitude below values commonly used in the industry. Rather, it is straight-forward to show that, neglecting resistance, the proper figure of merit for switching the maximum gradient over a given sample diameter d_S and length h_S in the minimum amount of time with a given amplifier power (VA product) is the ratio of gradient magnetic energy in the sample to total gradient energy [3]. Dropping a constant coefficient, we designate this as the dimensionless gradient *switching efficiency*, η_S, in SI units:

$$\eta_S = \frac{\alpha^2 d_S^3 h_S^2}{\mu_0 L} \tag{60.1}$$

where α is the *gradient gain* (T/Am) or coefficient (also called "efficiency" by some authors), μ is the permeability of free space, and L (H) is the total inductance. In large, high-power gradient systems, η_S is one of the most important parameters because the amplifiers and their operations cost are both greater than the cost of the gradient coils. For actively shielded gradients, η_S depends strongly on the ratio of the separation distance between the shield and gradient coils to the gradient coil diameter. It is also dependent, but to a lesser extent, on the maximum allowable coil length, which often is constrained for rf lead length or sample-access reasons. This switching efficiency ranges from 12% to 35% for most state-of-the-art shielded gradients for larger samples, where sample diameter is about 70% to 85% of the gradient coil diameter, but η_S is less than 3% in some of the older MRI designs and in many gradients designed for high-resolution NMR of small samples.

For microscopy gradients, the *IR* voltage drop in the windings at peak gradient strength is often comparable to the peak amplifier voltage, so eqn. (60.1) has limited utility, and DC efficiency (discussed shortly) is usually more important. There is yet another reason for the limited value of eqn. (60.1) in microscopy. With small rf coils where sample losses are negligible, *sensitivity* suffers if the external rf shield diameter is less than ~ 2.5 times the rf coil diameter, and resolution is usually limited by sensitivity here. Thus, one must use a relatively large gradient coil for best resolution and accept its amplifier requirements. Switching efficiency of the gradient coil is then best characterized simply by the ratio α^2/L, except in the case of very small coils, as noted later under the discussion of amplifiers.

60.2.2 Impedance Options

The coil designer has considerable control over L, α, and R [4]. For given dimensions, the gradient gain is proportional to the *number of turns n,* and the *inductance* is proportional to n^2. The resistance is also approximately proportional to n^2 and inversely proportional to the copper mass. By varying the thickness of the layers, the cross-section of the conductors, the number of layers, and parallel or series interconnections of the four

quadrants, the designer has a wide range of control over these three parameters, whether using etched foil or wire, without serious effect on important figures of merit. This allows optimal use of various amplifiers.

For a given switching efficiency and size, the rise time is determined by the gradient amplifier power (VA product) and *impedance matching*. The two halves of the gradient coils, which have precisely equal resistance and inductance, may be wired independently so that they may be connected either in series or in parallel. The coil parameters in Table 60.1, for example, are listed for the low-impedance (parallel) option. Switching to the series configuration may improve the impedance match and increase the peak gradient, but rise time to a given gradient is increased – gradient gain is doubled, resistance and inductance are multiplied by four, and η_S is unchanged. In some coils, this is user-switchable, and in some coils it is dynamically switchable to allow faster rise time with amplifiers of lower continuous power rating [5].

Matching the DC resistance of an optimized coil to the design load resistance of the amplifier for maximum output achieves maximum continuous gradient (assuming it does not exceed the coil's rating), but this is seldom the preferred choice. Rise time is improved by reducing the coil's impedance relative to the power-match optimum, but the extent of the mismatch must be limited by its effect on peak gradient. Another complication is that optimum power-match impedance for most amplifiers at pulse lengths under 1 ms is less than that for very long pulses. Thus, impedance matching in gradient coils is not a well defined concept, but simply reflects the emphasis on rise time vs. peak gradient strength. See section 60.3 for more comments on amplifiers.

60.2.3 Gradient Uniformity (Differential Linearity)

A key question is how much non-linearity is to be allowed in the sample volume, as a 10% increase in d_S and h_S in eqn. (60.1) increases η_S by over 60% for a given gradient coil. It is not uncommon to define *linearity* as the relative error in *actual field* (generated by the gradient coils) at the surface of the sample region compared to the *target field* that would be measured if the gradient had been constant (Turner [6]), regardless of the linearity along the path to the target field. The standard formulation of the Turner definition essentially weighs errors inversely in proportion to their distance from the center of the sample [7]. With this definition (which was generally used in early works), it is easy to achieve linearity under 2% even though the gradient in many places throughout the sam-

ple may be less than half the mean value and the field may not even be monotonic. Figure 60.1 shows a typical curve for a transverse gradient field $\boldsymbol{B}_G$ near the axial ends of the sample region and explains the common "telescoping" or compressing effect in this region. (The opposite curvature was typical near the equatorial plane in early designs.) Note that the field error at point x is zero, but the gradient error is large except near $x = x_1$.

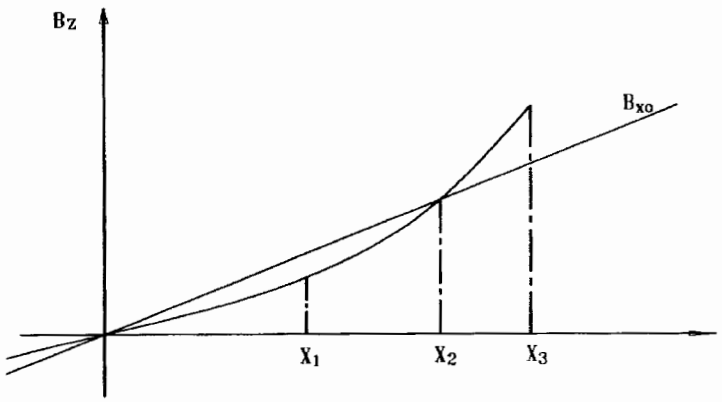

Fig. 60.1: Typical transverse gradient field near the end of the sample region.

A more useful specification is gradient non-uniformity (also called *differential linearity*) – i.e., relative root-mean-square (rms) *local deviation* σ of the gradient from its mean value throughout the sample volume [4,7,8]. This is still not unambiguous, as it depends on the number of elements examined within the imaging region. (Using fewer elements averages localized errors. We typically look at over 1500 elements per octant of the sample region.) The linearity also depends on whether one is specifying a *spherical* or a *cylindrical* sample region – which gives 50% more imaging volume. While some authors have used maximum errors, most have used rms sums and a few have used weighted rms methods in which the error is weighted by a function that somewhat reflects the significance of the location in typical images.

The above variations allow numerous definitions of gradient accuracy, and most have probably been used at one time or another. Most authors prior to ca. 1994 (and several as recently as 1996) appear to be using definitions similar to number 8 or 9 below when not otherwise specified. In order from most stringent to least stringent, the more common gradient accuracy definitions are:

1. Maximum local gradient error throughout sphere or ellipsoid
2. RMS local gradient error throughout a cylinder
3. RMS local gradient error throughout sphere or ellipsoid
4. Weighted RMS local gradient error throughout cylinder
5. Weighted RMS local gradient error throughout sphere or ellipsoid
6. Maximum field error on surface of cylinder
7. RMS field error on surface of cylinder
8. Maximum field error on surface of sphere
9. RMS field error on surface of sphere or ellipsoid

Note that the last four only address position error at the boundaries of the image. Another minor variation on the ellipsoid is to use a slightly chamfered cylinder. We generally ignore a small (10% of radius) chamfer on the edges of the cylinder, as it is not likely that this region will have sample of interest, or be able to be shimmed, or have usable $\boldsymbol{B}_1$ homogeneity.

Local gradient coils with rms relative deviations σ above 40% have been used by the major MRI manufacturers and have not posed serious problems in distortion correction [9–11]. However, for microscopy, it may be better to specify the size of the 4% and 10% *cylindrical* regions, as the gradient amplifiers are relatively inexpensive and sophisticated distortion correction software is not available from all microscopy vendors. In practice, distortion from $\boldsymbol{B}_0$ *susceptibility* effects is usually more significant than distortion from gradient non-linearity in microscopy, irrespective of gradient coil design, as the sample is usually less than half the gradient coil diameter. General methods have recently been demonstrated that appear to be quite robust in dealing with a variety of sources of *distortion*, including gradient non-uniformity, susceptibility, temporal distortions in gradient waveform, and $\boldsymbol{B}_1$ inhomogeneity [10,11]. As image post-processing becomes more widely available in microscopy, we expect future trends to be in the direction of greater gradient non-uniformity so that higher continuous ratings and efficiencies (both switching and DC) and lower nerve stimulation can be achieved – a point we will return to later.

60.2.4 Gradient Null Point

In many microscopy applications, especially where the sample is quite long compared to its diameter (mice, rats, plants, etc.) and in human head MRI with local gradient coils, the location of the nearest *gradient null point* (*field inflection point*, z_0) is more important than linearity, as signal from this region begins folding back and there is nothing that can be done to improve a multi-valued function by post-processing. Most conventional inductance-minimization optimizations put this point (which is located on the z axis) at an axial distance from the center just 20% to 30% beyond the edge of the nominally linear region. In our recent microscopy optimizations, the gradient null point is pushed axially outward an *additional* 30% to 40% for all gradients (see Table 60.1). This makes it much easier to insure that rf sensitivity from a body coil is low enough in this region to avoid *fold-back* problems with long samples. While this also helps linearity near the center at the axial ends, it comes at a price – primarily in reduced η_S and increased B_0 eddies. It also requires an increase in overall coil length, which may compromise multi-nuclear rf tuning, but it is usually justified for the above applications.

60.2.5 Eddy Currents and Recovery Time

The external fields from unshielded gradient coils may induce enormous currents, similar in pattern to the gradient windings but of opposite sign, in the external construction materials. The time constants for the major *eddies* from unshielded gradients in moderately large magnets are typically characterized by a relatively fast component (several milliseconds) from the stainless cryostat, a moderate component (tens of milliseconds) from the first copper radiation shield (78 K), and a slow component (hundreds of milliseconds) from the cold (~ 20 K) radiation shield. In small magnets, the time constants are proportionally smaller. The typical magnitudes of the induced gradient fields are about 60%, 20% and 4% for coil/bore diameter ratios of 0.9, 0.7 and 0.5 respectively. The time dependence imparted by the eddies may be largely compensated either in hardware or in software by multi-exponential *eddy current compensation* (*ECC*), which is achieved by simply applying the proper combination of high-pass filters to the gradient waveform [12], but this does not address cryogen boiling from I^2R heating of the shields and acoustic modes in the shields. Moreover, power dissipation in the amplifier output devices is increased dramatically, and resistance changes from eddy heating of the shields make the compensation strongly dependent on the pulse sequence

and history. More effective post-processing methods based on wavelet transforms, which eliminate eddy current effects under many conditions [13], have recently been demonstrated, but still one is left with the effects of strong acoustic modes and heating in the radiation shields. The best solution is to start with external *active shielding* coils [1,14,15].

A *shielding factor* (*SF*) can be defined as G_P/G_E, where G_P is the gradient produced by a long square current pulse at the rated peak current and G_E is the mean residual first-order gradient in the sample region shortly after the current pulse vanishes. It is probably more customary to characterize shielding effectiveness by the relative residual linear gradient or G_E/G_P. *SF* depends sharply on the distance to the cryostat cold shield; in microscopy, we typically assume a cryostat cold shield radius 40% greater than the gradient shield radius. When the ratio of magnet bore diameter to gradient coil diameter is greater than ~ 2, shielding is often not required, even for fast waveforms with relatively large *residual gradients* if the compensation is sufficiently accurate and complete – for example, with asymmetric torque-balanced unshielded gradient coil designs [4,16]. (It should be noted that the above referenced asymmetric designs assume a uniform $\boldsymbol{B}_0$. More accurate designs that take into account the non-uniformity of the external $\boldsymbol{B}_0$ have also been proposed, but they have a large dipolar far-field component and hence generate larger eddy currents.)

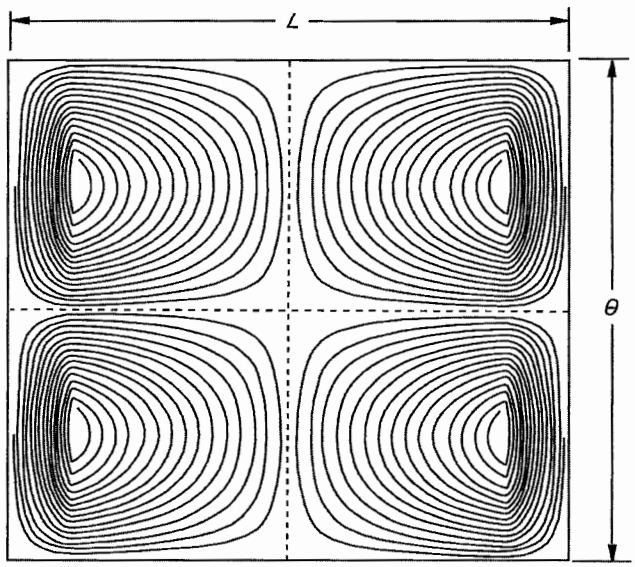

Fig. 60.2: The Schenck transverse "finger-print" gradient coil.

The classic, etched 'fingerprint' design of John Schenck et al [2], as illustrated in Fig. 60.2, achieves high η_S and linearity, and it can easily be shielded, as shown by Pete Roemer et al. [14]. The first-order cryostat eddies from minor shielding errors have time constants about an order of magnitude less than $\boldsymbol{B}_0$ eddies and thus may be easily compensated or sometimes ignored. However, the high current-concentration ratio of the inductance-minimized design limits power handling and exacerbates acoustic problems, as will be seen later. Another minor problem with low-inductance coils of this type is that the high-frequency current distribution in the wide portions of the foils is quite different from the low-frequency distribution [17]. That is, eddy currents are generated within the gradient and shield conductors on the driven axis and on the orthogonal axes, although these time constants are quite short.

While the dominant eddy from an unshielded gradient is always the respective linear component, the largest residual eddy in 3-axis shielded gradients is usually the $\boldsymbol{B}_0$ *eddy* from manufacturing tolerances in the z-gradient [18]. Low-amplitude, slow $\boldsymbol{B}_0$ eddies (tens or hundreds of milliseconds) are induced in the magnet shields primarily from minute variations in coil diameters along the axis or from axial registration errors between the gradient and shield coils. Fast components (under 100 μs) may arise from axially asymmetric distributions of metallic structures in probes, cryostat shields, or shim sets. Whatever the source, they can easily be compensated by a time-dependent correction (a derivative of the gradient signal) applied to a B_0 shim coil. The correction is normally quite small (usually 0.1 to 1 ppm, depending strongly on the shield/gradient coil diameter ratio and manufacturing processes). It is often easier to add a separate, light-weight $\boldsymbol{B}_0$ coil to the gradient coil assembly than to apply the correction to the existing room-temperature Z_0 shim coil driver. Another approach is to add a time-dependent correction to the receiver reference frequency or to the FID phase [19].

When ECC (high-pass filters or "*pre-emphasis*") is not available (as on some older NMR spectroscopy systems), the gradient in a perfectly shielded gradient coil driven by a *constant-voltage* amplifier will decay exponentially with a time constant given by L/R_E, where R_E is the resistance of the gradient coil. This time constant is often tens or hundreds of microseconds for small coils and milliseconds for large coils. When the coil is driven by a *constant-current* (*CC*) supply, the appropriate resistance is the small-signal amplifier output impedance, which is infinite for the ideal CC amplifier. However, the output impedance in real, high-power CC amplifiers varies from ~100 Ω to perhaps 10 kΩ below ~100 Hz and decreases inversely with frequency above ~ 500 Hz, which limits actual L/R time constants under CC to typically 1 to 100 μs. More comments about amplifiers will be made later.

Interaction between the rf and the gradient coils makes rf tuning unpredictable unless a full, symmetric *rf shield* is included between the gradient coils and the rf. Some prior rf shields have introduced image artifacts because of acoustic resonances, some have caused eddy current problems for fast gradient techniques, and many have severely degraded rf coil performance [20,21]. A surprisingly large number of patents have been issued for various slit patterns that minimize gradient interactions while providing rf shielding (generally with high loss and over a narrow band), but their utility is primarily limited to large gradient systems where gradient power loss otherwise can be several kilowatts. For microscopy, where rf tuning flexibility and unloaded rf sensitivity are paramount, the best approach is a full cylindrical copper shield about three skin depths thick at the imaging frequency (20 microns at 100 MHz, for example) just inside a somewhat thicker shield of low-conductivity alloy at the largest possible diameter. Even then, sensitivity is improved about 20% (for a 12 mm rf coil at 400 MHz, for example) when the rf shield-to-coil diameter ratio in increased from 1.5 to 1.8.

The time constants and power dissipation of the eddy currents induced in the rf shield depend as much on the distance between the gradient coil and rf shield as on the shield conductance. There has been some confusion in the literature about the time constants and significance of these eddy currents in echo planar imaging (*EPI*). The appropriate *L/R* comes from the leakage inductance between the coil and the rf shield and the loop resistance in the rf shield. Minimizing the separation distance minimizes the rf shield time constant (by reducing leakage *L*) but increases power loss during switching. For small coils with closely spaced continuous rf shields as described above, this time constant can easily be under 1 μs, and the gradient attenuation (a simple resistive loss) will be quite acceptable up to at least 10 kHz. The increased gradient power loss at high frequencies is distributed between the rf shield and the stainless steel bore tube of the cryostat, as the presence of the rf shield spoils the gradient shielding at higher frequencies. The time constants of eddies in the stainless steel tube are also very short.

More significant (but still minor) internal eddy currents arise from the interactions between the three orthogonal gradient coils when heavy windings are used, as the skin depth in copper at 6 kHz is only 1 mm, and there are indications that some future imaging modalities (e.g., transverse acoustic strain elastography) may benefit from gradient frequencies at least this high. Some improvement is obtained by restricting the z windings from the narrow window regions of the transverse gradient coils, as their transverse DC fields are highest there. This restriction is somewhat detrimental to z-gradient linearity,

but appears to be justified for EPI, as *ghosts* generated from eddy currents above first order are not well addressed by standard ECC and calibration scan methods, although more sophisticated methods appear to work better [22].

60.2.6 DC Efficiency and Continuous Gradient Rating

Surprisingly, almost all prior optimizations are completely silent on what is coming to be recognized as the most important problem in microscopy gradient optimization – the *continuous gradient* rating. The few prior works that recognize the importance of resistive losses in the coil usually calculate this parameter after, and essentially independent of, the coil optimization [4,17]. Yet, if resistive losses can be kept low enough, forced air cooling is often adequate, which simplifies experimental setup and improves reliability. Also, high-velocity water cooling may cause image artifacts of microphonic origin.

Low frequency (LF) or *DC efficiency* η_L may be shown to be given by the following expression [3]:

$$\eta_L = \frac{200\,\alpha^2\, d_S^3\, h_S}{\mu_0\, R_E} \tag{60.2}$$

where R_E is the coil resistance in ohms and the constant coefficient has units of m/s. This expression stands apart from the rest of our efficiencies in that it is dimensionless only by virtue of the constant's units, and it implies that cooling problems become more severe with smaller gradient systems. Since α is proportional to n and R_E is approximately proportional to n^2 for a given coil geometry and copper mass, η_L, like η_S, is essentially independent of the number of turns. LF efficiency increases with conductor mass, but it is particularly sensitive to conductor thickness in regions of high surface current density. For reliability, cooling effectiveness at local hot spots near the ends, where surface current density is higher by factors of two to four in conventional optimizations [2,4,6,7,14–16,23,24], is even more significant than total LF efficiency. Because of the importance of reliability we typically limit *current concentration ratios* (volume density ratios) to about a factor of 1.4.

Multi-layer wire windings in critical areas combined with crescent coils [3] have permitted high-gain designs with higher LF efficiency and much lower current concentration than is possible with etched or laser-cut foil patterns, particularly in small coils

with extended imaging lengths. This is only partly because the use of enameled wire and the elimination of composite substrates allow a higher ratio of copper to insulator in critical areas. Among other factors, the total thickness of the windings in our gradient coil for a 3-axis microscopy set is about 15% of the radius in regions of maximum current density, which appears to be 2 to 7 times thicker than most other designs. Even with this much copper, internal eddy currents may be kept small by proper attention to symmetries and transparency in critical areas. For example, we typically measure inductance at 15 kHz before the rf shield is added to be only ~ 2% less than that at 4 kHz.

As with switching efficiency, the above LF efficiency is less meaningful in microscopy applications where the sample is quite small compared to the gradient coil; the simple ratio, α^2/R_E, is more useful. This "DC" ratio, the current concentration ratio, and the cooling effectiveness determine the maximum continuous gradient. Unfortunately, the cooling effectiveness is not easily reduced to a simple expression of well-defined variables and it is often highly dependent on localized coolant flow rate – whether air or water. Thus, it is essential that a maximum continuous gradient (meaning many months, DC) be determined by the manufacturer for a specified coolant flow rate for the specific model.

Some manufacturers have confused continuous gradient ratings by calling a rating for one *second* a continuous rating, even though many microscopy applications require hours of run time and *thermal time constants* in microscopy coils are typically 3 to 30 minutes. Since thermal time constants are usually at least three orders of magnitude greater than the gradient pulse length, maximum duty cycle (at least down to 0.3%) is simply $(i_{RMS}/i_P)^2$, where i_P is the pulse current and i_{RMS} is the true continuous rating, assuming the coils and leads are very well secured. Continuous ratings are normally given for a single, driven axis and must be lowered about 10% to 30% when two or three axes are driven hard simultaneously.

60.2.7 Water Cooling

Using an *alumina-ceramic* gradient-coil former (rather than a plastic composite) increases stiffness by nearly two orders of magnitude, which gives exceptional dimensional stability for improved gradient accuracy and greatly reduces low-frequency noise and vibration, as discussed later in more detail. However, its greatest advantage may lie in the simplification it permits in cooling [3]. Its very high thermal conductivity helps

equilibrate hot spots and allows efficient cooling via a thin water jacket on the inside of the gradient coil. This approach has proven effective in several small microscopy gradients sets (up to 1000 G/cm) and PFG coils up to 2000 G/cm. Using an internal *water cooling* jacket has the additional advantage of keeping the internal rf shield at a relatively low temperature (below room temperature), thereby reducing its contribution to *Johnson noise* in the rf coil. The efficient flow geometry of an internal water jacket permits operation at reduced pressures and minimizes turbulence for reduced microphonics, but excellent results have also been achieved with water directly flooding epoxy-coated conductors. The most significant limitation to heat removal in multilayer windings is the polymeric insulation between layers, which must withstand a high-voltage (often >300 V) isolation test, but this limitation becomes even more severe with composite substrates between etched coils. Water cooling of microscopy coils typically increases the continuous gradient rating by a factor of two to three, which is comparable to the improvement that is possible by simply optimizing for high DC efficiency.

Water cooling of large gradient coils has often been implemented by running water through copper cooling coils bonded over the hot spots on the gradient coils. Here, the cooling coils, in addition to requiring low thermal resistance to the windings, must satisfy a rather stringent serpentine path requirement: To avoid coupling to the gradient transients, they must be magnetically orthogonal to the X, Y, and Z gradient coils. Moreover, since they are located in the near-field region, a detailed time-dependent electro-magnetic FEA model is required to achieve sufficiently low internal eddy currents. This is the only time orthogonality becomes a real issue in gradient design.

With expensive apparatus, it is standard procedure to use an isolated cooling loop of distilled or deionized water and a commercial heat exchanger connected to the external water supply. Standard pumps, over-temp, coolant flow, and coolant-level sensors are required along with a simple control system.

60.2.8 Force Cancellation and Acoustic Efficiency

All symmetric gradient designs have zero net torque and zero net force in a uniform external field, and this is essential unless substantial effort is put into magnet and gradient structure reinforcement and safeguards. However, there are always large local forces and torques within the coil system that cause localized deflections, vibration, and *acoustic noise* [25]. Moreover, most failures we see are fatigue-related (inadequately secured

conductors that are too thin in the radial direction) and only indirectly heat related – the low-frequency vibrations increase sharply above the glass-transition temperature of the coil encapsulant or coil-form matrix.

While it is desirable to eliminate acoustic noise in whole-body MRI for reasons of patient and operator comfort and safety [26], another reason is that some of the image artifacts attributed to eddy currents in actively shielded gradient coils are more likely acoustic in origin. We have compared the recovery time of a conventional (minimum inductance) microscopy gradient coil with *SF* (shielding factor) greater than 200 but with high acoustic efficiency to a crescent-type coil (at comparable $B_0 d_S$) with $SF < 70$ but having ultra low acoustic efficiency. The former had recovery time (to field homogeneity of 0.2 ppm) greater than 20 ms. The latter had recovery time less than 20 μs, which is three orders of magnitude improvement! Moreover, EPI ghosts are often completely undetectable with crescent coils, even without employing advanced artifact reduction techniques.

Four ways of addressing the acoustic noise problems are currently being pursued by various groups: (1) ear plugs and enhanced *acoustic absorption* in gradient construction [26,27], (2) active acoustic cancellation headphones, (3) increased *coil-form stiffness* [28], and (4) *force-cancellation* to minimize electro-mechanical *acoustic efficiency* [3,29,30]. The last of these approaches is the most beneficial in improving image quality, as the reduction in the efficiency of generating acoustic energy will reduce the efficiency of the acoustic energy coupling back into the magnetic field and altering it. This acoustic efficiency is a complex function of frequency, but some low-frequency and high-frequency approximations can be expressed in simple form. The electro-mechanical efficiency – which we desire to minimize – is defined as the ratio of peak mechanical energy (potential plus kinetic) of the coils to electromagnetic gradient energy in the sample region. The acoustic problem may be divided into three regimes: low frequency, near fundamental resonances, and high frequency.

The fundamental transverse bending mode of a uniform, medium-walled cylinder, heavily loaded at both ends (the typical case), is the mode most strongly excited in the standard, torque-balanced transverse gradient coil. Its angular frequency ω_b is approximately

$$\omega_b \approx \frac{5 r_f c}{h^2} \tag{60.3}$$

where r_f is the mean cylinder radius, h is the cylinder length, $c = (Y/\rho)^{1/2}$ (the velocity of transverse acoustic waves), Y is *Young's modulus* of elasticity, and ρ is the mass density. This assumes that the multi-layer coil-form/coil structure is solidly laminated and may be characterized by an effective Y and an effective ρ. For a typical microscopy fiberglass gradient-coil form, 80-mm in diameter, covered with copper windings, $\omega_b/2\pi$ is in the range of 300 to 1500 Hz.

The bending stiffness k_b (N/m) of a cylinder with wall thickness w (where $w << r_f$) is approximately

$$k_b \approx \frac{100 Y r_f^3 w}{h^3} \tag{60.4}$$

The mechanical energy U_M in the LF regime (well below ω_b) is approximately

$$U_M \approx \frac{F_b^2}{2k_b} \tag{60.5}$$

where F_b is the Lorentz bending force near the center. By using ceramic coil forms (very large Y) or by placing stiffening struts in the space between the gradient-coil form and the shielding-coil form (effectively increasing w and Y/ρ), k_b and ω_b are increased and U_M may be reduced to a negligible level throughout the LF regime. Similar results are readily obtained for the axial gradient built from distributed Maxwell pairs.

Partially filling the space between the gradient-coil form and the shielding-coil form with rigid composite struts has the additional beneficial effect of reducing LF acoustic efficiency by providing a rigid mechanical coupling (of length much less than an acoustic $\lambda/4$) between oppositely directed forces, thereby achieving partial force cancellation [28]. For Roemer and related coils with typical shield/gradient ratios, the force cancellation is about 30%, and this approach now appears to be common practice.

Even with ceramic coil forms and rigid struts between the gradient- and shielding-coil forms, it is not possible to make ω_b large enough to ensure that mechanical resonances will not be excited by the high-frequency components in fast-switching pulses. Hence, it is also necessary to look at the resonant and high-frequency acoustic regimes.

It may be shown that for shielded *Golay coils* [31] of the type shown in Fig. 60.3 in external magnetic field B_0, the acoustic efficiency in the high-frequency regime η_{mh} is approximately (in SI units),

$$\eta_{mh} \equiv \frac{(r_g B_0 t_g)^2}{2\eta_S \mu_0 m_C (r_S - r_g)} \tag{60.6}$$

where r_g is the coil radius, t_g is the gradient pulse length, m_C is the effective mass of the coils, and r_S is the shield coil radius. Note that the efficiency in eqn. (60.6) is independent of coil-form stiffness but is inversely proportional to *coil mass*. This efficiency normally increases with r_g because t_g increases faster than m_C/r_g.

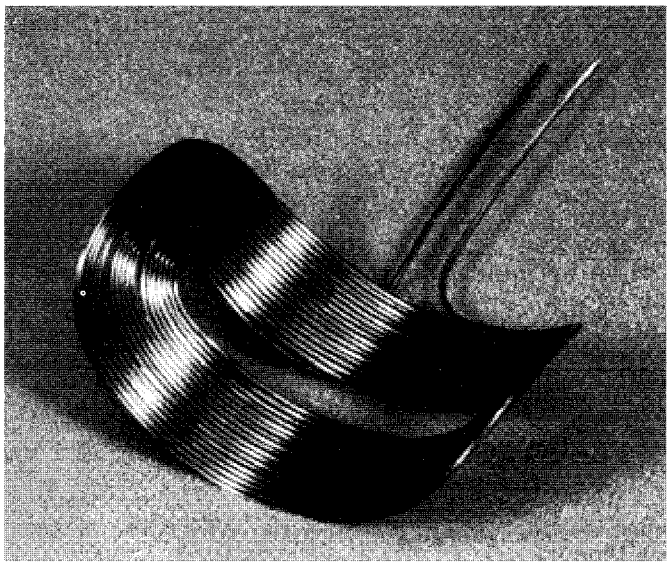

Fig. 60.3: Heavy, wire-wound Golay coils.

The above acoustic efficiency may range from less than 1% to more than 1000% – meaning the acoustic energy may be more than 10 times the useful gradient magnetic energy. (With a little reflection, this should not come as a surprise, as the gradient field energy within the sample can easily be less than 5% of its total magnetic energy, and highly efficient loudspeakers are driven by voice coils in fields of about 1 T.) As the pulse repetition frequency approaches ω_b, eqn. (60.6) under-estimates acoustic efficiency by a factor comparable to the mechanical Q, which may exceed 10. The increased acoustic motion from the high-current-density regions in inductance-minimized etched, laser-cut, or even wire designs can lead to rapid failure at high fields. Note that it is the volume

(not surface) current density and other tightly coupled mass that are important here. Recall that volume current density is also the more important (but often ignored) factor in continuous gradient rating.

There are two methods of reducing HF coil motion: (1) Increasing the effective coil mass, especially where volume current density is high; and (2) Increasing the efficiency of force cancellation, which may increase the constant in the denominator of eqn. (60.6) from 2 to 20. Force cancellation requires coil geometries not constrained to simple cylindrical surfaces [29,32,33]. Also, these coil geometries shift the acoustic response to the low-frequency regime, where the electro-mechanical efficiency is several orders of magnitude lower and is inversely proportional to stiffness and other geometric factors. Increasing coil-form stiffness, on the other hand, will *increase* coil motion of the dominant HF modes. This seemingly counter-intuitive result has been well understood for many decades in the loudspeaker and sonar industries [34].

Although manufacturing of the above referenced force-cancelled approaches for 3-axis systems may appear impractical, we have developed related geometries, crescent coils, with similarly low acoustic efficiencies that are readily manufacturable [3]. Moreover, the crescent coils may be readily combined with golay coils to permit much higher DC efficiency while still retaining 90% force cancellation in the critical, central region. This approach to force cancellation, which we will return to in more detail in a later section, typically gives a 25 to 35 dB reduction in vibration and noise with dramatic reductions in EPI ghosts while permitting higher continuous gradient ratings – largely by eliminating hot spots. The conventional approach, on the other hand, to MRI noise reduction (adding absorptive materials) seldom reduces broadband acoustic noise by more than 11 dB [26] and may complicate access, thermal, background, and tuning problems.

60.2.9 Nerve Stimulation

For research groups planning to use fast gradient techniques on relatively large, live animals, *nerve stimulation* is likely to become an issue, as it is presently the critical, limiting factor in whole-body MRI [35]. Force-cancelled designs have been shown to have lower nerve stimulation than traditional designs [32] because of lower transverse fields and lower peak field regions (which is the critical regulatory criterion).

If EPI or related techniques are eventually to be used in whole-body MRI at high fields, it will be necessary to develop the techniques with gradients of high non-uniformity and improved distortion correction software [10,11], as this is the only way to further reduce maximum field within the subject for a given mean gradient in the region of interest. Even in microscopy, it may be desirable to trade some gradient uniformity for reduced nerve stimulation and enhanced switching performance. We find, for example, that a degradation in gradient uniformity from 10% to 12%, gives a 5% to 10% decrease in rise time and nerve stimulation is decreased by about 10%.

We have quantified peripheral nerve stimulation by indicating B_M/B_G, where B_M is the largest change in field magnitude, averaged over any area equal to 10% of the sample cross-section, generated by the gradient coils anywhere within an arbitrarily long cylinder of diameter equal to the maximum sample diameter, and B_G is the maximum z component of the gradient field within the sample region for an ideal gradient field having perfect uniformity.

60.3 Gradient Amplifiers

The matching of the gradient coils to the gradient *amplifier* with peak current capability i_P and peak output voltage V_P is characterized by the following parameters: peak gradient $G_P = \alpha i_P$ (when $i_P R_E < V_P$) and *rise time* τ_r from 5% to 95% of G_P. For an amplifier with zero rise time,

$$\tau_r \cong \frac{L\, i_P}{V_P - i_P\, R_E/2} = \frac{L\, G_P}{\alpha(V_P - i_P\, R_E/2)}, \tag{60.7}$$

when $i_P R_E < V_P/2$, which is often not satisfied in microscopy. In fact, $i_P R_E$ is often not much less than V_P, in which case $G_P = \alpha V_P/R_E$. The rise time of the amplifier (typically 4 to 6 μs) must be added to the above for total rise time, and more accurate values may be readily obtained by solving the appropriate differential equations when the above approximations are not adequate. The rise time increases linearly with G_P for small values thereof, but τ_r increases exponentially as the limit is reached.

As previously mentioned, *settling time* to within 0.2% of the final value is usually greater than rise time in microscopy. With well designed gradients, this is primarily

determined by amplifier bandwidth and ECC flexibility unless pre-emphasis is not used, in which case it is determined by output *impedance* in CC mode. Clearly, fast switching requires high voltage, and high gradients require high current. In microscopy coils, the high values of gradient gain (α) make DC *drift* and noise critical specifications, and balanced input (or optical isolation) is absolutely essential. The use of crossed-diodes (even Schottkey type) in the output for noise squelch is generally not an acceptable alternative – especially for multiple-quantum techniques, which depend on a linear response to very low levels. Extra high output impedance is beneficial for fast settling of inductive loads without pre-emphasis, but it is even more essential for minimizing the coil heating effects on gradient magnitude, as a 30 °C increase in coil temperature reduces coil current by 10% with a constant-voltage amplifier. In some diffusion experiments, the integrated gradient in bipolar pulses must be matched within 10 ppm, which is quite difficult with amplifier output impedances less than 1000 times the coil resistance. The Highland™ amplifiers excel in this regard, although their low VA product (~ 1000 W) imposes serious limitations on gradient strength and rise time with all but the smallest gradient coils – i.e., settling time may be less than rise time.

One reason for the common perception that minimizing inductance is a primary objective is that linear power amplifiers become much more expensive (per watt) for V_P above 300 V. However, they also become more expensive for i_P above 250 A, and 1000 V dual-level amplifiers are becoming available. Switch-mode amplifiers become more cost-effective for VA above 20 kW (especially above 300 V) and have been used very successfully in conventional whole-body MRI, but their low bandwidth (~5 kHz) severely limits their utility in microscopy, EPI, and *elastography* using MRI with transverse acoustic waves [36]. An alternative approach that appears to combine the best of both approaches is a linear amplifier powered by a "piggy-back" power supply (a low-voltage supply riding on a high-voltage supply) that is able to efficiently provide high voltage at low current and low voltage at high current with virtually no switching noise and minimal charge-up delay [37].

Transmission line inductance (typically 1 μH/m) in the cables between the amplifiers and the coils becomes significant for coil inductance below 100 to 200 μH. The use of cumbersome low-impedance cables (0.2 μH/m) is necessary with very-low-inductance coils. Hence, optimum coil inductance is typically 50 to 200 μH except for whole body EPI, where somewhat lower values may be needed until higher-voltage supplies become more readily available.

For EPI with *tuned gradients*, $\eta_S Q_E$ is a useful electrical efficiency figure of merit, where the gradient coil electrical quality factor Q_E (typically 2 to 4 for large microscopy coils at 2 kHz) is measured at the read frequency. In this case, transmission line losses and rise time considerations essentially vanish. One simply matches the amplifier design load impedance to $\omega L Q_E$. The amplifier cost may be cut by nearly an order of magnitude, even though Q_E is rather low. However, tuned gradients are unsuitable for other fast gradient methods, such as spiral scan, and are not even well suited for EPI, as trapezoidal waveforms are better than sinusoidal.

60.4 The Crescent Coil Design

At least three groups (Mansfield, Roemer, and Doty) were independently working on actively shielded gradient coils by 1985; and in early 1991, we began exploring approaches to solve motion-related artifacts in high-field microscopy coils and to increase duty cycle. The crescent coil design which evolved along with the dimensionless analysis has proven to be extremely effective in controlling the vibrational problems otherwise encountered in high-field high-performance microscopy.

The crescent gradient coil design is described in more detail elsewhere [3], but a brief description is provided here. A high-conductivity ceramic coil form is used to improve rigidity and cooling effectiveness for 3-axis MRI gradient coil configurations on a single

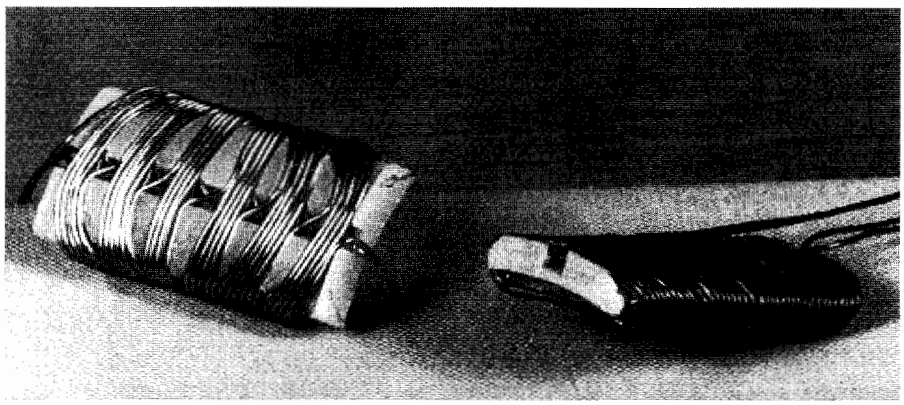

Fig. 60.4: Crescent coils – zero net torque when aligned with B_0.

cylindrical coil form aligned with B_0. Normally, eight crescent-shaped, axially aligned solenoid-like coils, as shown in Fig. 60.4, are attached around the perimeter, bisecting the equatorial plane. The four crescent coils aligned on an X or Y axis contain windings for the X or Y gradients respectively. The four *crescent coils* between them contain windings for both axes with proper phasing of the X and Y coils.

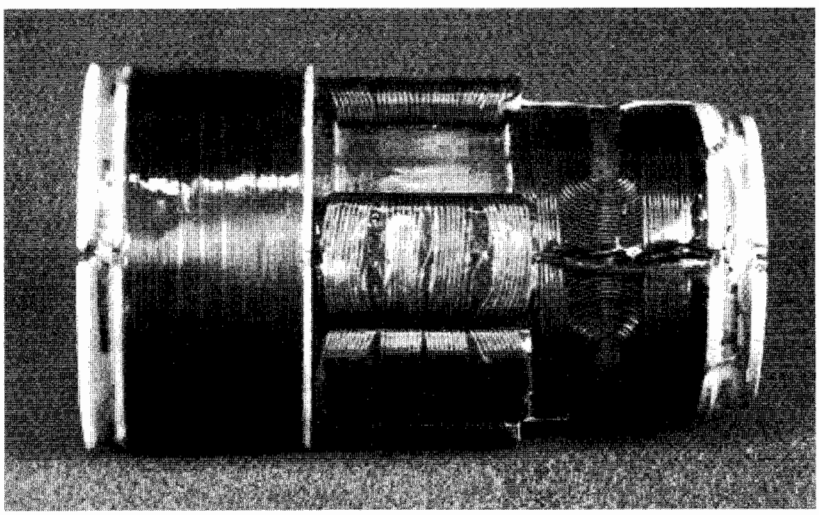

Fig. 60.5: Partially assembled crescent gradient unit.

The design is similar to the "*Concentric Return Path*" concept by Brey, Andrew, and co-workers, the force-cancelled arc-loops of Mansfield and co-workers, and the reduced-nerve-stimulation design by Frese et al. However, the first key improvement (which makes this design manufacturable) is that fewer 3D coils are required, and they may be independently wound, encapsulated, and tested prior to mounting on the main cylindrical form. The second key achievement is that η_S and η_L may be improved by nearly an order of magnitude (compared to the alternative force-cancelled approaches) by (a) using inclined crescent windings that reduce the surface current density on the outside relative to that on the inside, (b) by combining the crescent coils in an optimized way with heavy Golay coils, and (c) by permitting higher surface coverage by the windings. The third improvement is that heat removal in regions of high power density is much more effective; and the fourth advantage is that by properly controlling the current densities on the crescent coils, the severe over-shielding near the center that characterizes other force-

canceled designs is eliminated. It is usually also beneficial to add minor transverse shielding Golay coils at each end, but power density there is very low so vibration is easily controlled and resistive losses are negligible. Figure 60.5 shows a mostly complete 50-72 gradient assembly (some shielding coils, one crescent coil, and some z-windings at one end are omitted for better clarity).

Some have suggested that using wire is inherently inferior to using etched (or laser-cut, or water-jet machined) foil patterns. One argument for machined foils is more control over surface current density, which helps a little with linearity and switching efficiency in most cases. Unfortunately, it also creates high-current-density regions which limit the maximum gradient rating and are the source of most of the acoustic noise. The combination of wire-wound crescent coils with wire-wound golay coils allows adequate control over current densities for comparable linearity and switching efficiency with the advantages of greater robustness, higher continuous and pulse ratings, much less vibration, reduced internal eddy currents with heavy windings, less image fold-back, and less nerve stimulation. It often appears initially that machined foil patterns permit easier manufacturing. Indeed, considerable effort has been required to develop effective manufacturing processes for precision crescent coils and heavy-gage golay coils. However, except for low power applications, we doubt that alternative approaches are significantly less costly. Finally, it has been suggested that etched coils are more precise, but it appears the crescent/golay coil approach achieves lower B_0 eddies, which is probably the best indicator of manufacturing precision.

Perhaps one reason this design has not been explored by other research groups is that it lacks the simple symmetries that are required for analytical solution. For that reason have never even attempted an analytical solution, although we have developed approximate parametric models. However, the fields, resistance, inductance, forces, torques, and gradients can easily be calculated by numerical methods from elementary laws (Biot-Savart equation, Ohm's law, and various basic relationships) for any set of conductors with known currents, from which the various dimensionless optimization efficiencies are easily calculated. Hence, our approach was to develop robust, flexible, easy-to-use software with simplex optimization capabilities and let the simple-minded computer go to work on it. We have not incorporated coil susceptibility calculations into the optimization, as we have not found this difficult to address separately from the rest of the optimization space. However, the software has also been found to have advantages in solving certain rf and susceptibility problems [38].

Using predominantly *dimensionless* parameters (a carefully weighted sum of η_S, η_L, σ, SF, and η_{mh}) with less weight on a few dimensioned variables (L, R_E, z_0, m_C) in the simplex optimization function makes it much easier to consistently arrive at a globally optimum solution that addresses all of the issues in MRI gradient coil design for different systems. Of course, trade-offs are a part of any optimization. For example, moving the nearest gradient null point z_0 further out and improving linearity come primarily at the expense of reduced switching efficiency. Increasing the continuous gradient rating comes from reducing current concentration ratios and increasing copper mass – which requires some loss in switching efficiency or linearity and increased manufacturing costs. It is difficult to fully incorporate all of the manufacturing constraints into the software, so an experienced engineer has to periodically apply additional constraints in guiding it to an optimal, manufacturable solution. However, one of the strengths of our computational approach is that discretization of current distributions after the optimization is not required, as wire dimensions and even end allowances are incorporated into the optimization from the very beginning.

The design typically ends up as follows: (a) the crescent coil length is comparable to the length of the high-homogeneity (4%) sample region; (b) the volume current density in the Golays is about 40% higher than in the axial crescent coils; and (c) the volume current density in the Golays is comparable to that in the diagonal crescent coils, as these coils require windings for both transverse axes. Also, the Golay coils typically (a) have axial length comparable to the length of the crescent coils, (b) have maximum subtended angles of about 176°, and (c) have window lengths about 4 times the wire diameter. The calculated performance parameters consistently agree within several percent with measured values, as shown in Table 60.1. For the standard supercon geometry, the data listed are for the two transverse axes, and the performance of the z-axis is considerably better. (Note that the second row is in the more familiar Gaussian units as preferred by most users.)

The design of the z-gradient will not be discussed in detail because it is rather simple in comparison to the transverse gradients for a cylindrical coil aligned with $\boldsymbol{B}_0$ and because it has been extensively discussed in the literature [39,40]. Briefly, low-density foil windings are laid down before the crescent coils are mounted in the central region, and additional, high-density z-gradient windings are placed over the x and y Golay windings at each end. Performance of the z-gradient based on these modified *Maxwell pairs* always exceeds that of the transverse gradients, and for that reason the main z windings are placed outside the Golays. However, this results in more cumulative radial

positioning errors for the z-gradient and hence larger $\boldsymbol{B}_0$ eddies, which may be addressed by a $\boldsymbol{B}_0$ correction coil or data processing [13,18]. An alternative under consideration is to lay the entire z winding down first, as this should allow the B_0 eddy from the z-gradient to be reduced to about that of the transverse gradients, although performance of the transverse gradients will be reduced by about 10%. (This will also reduce acoustic problems in the z-shield windings, which are presently the primary acoustic source in our coils.) The $\boldsymbol{B}_0$ eddy from a 10 ms x-gradient pulse of 10 G/cm in Doty model 50 - 72 W in an 89 mm magnet, for example, is usually less than 0.1 ppm with a time constant of about 15 ms.

Space also does not permit detailed discussion of numerous, critical, manufacturing details that can end up killing an otherwise excellent design. Chief among these are (1) wire routing to minimize lead stray fields, as they can be too complex to shield effectively, (2) copper surface preparation for adequate adhesion to the encapsulant, (3) wire forming and bend relaxation allowances, (4) precision bench testing during production to permit detection and correction of errors, (5) formulation of an encapsulant having high thermal conductivity, arc resistance, and bond strength, and (6) fluid-tight designs that permit access to and repair of some of the more failure-prone components, such as power and fluid connectors and bridging conductors.

60.5 Quadrupolar Gradients for use in Transverse $\boldsymbol{B}_0$

Before concluding, a few brief remarks will be made about the other class of high-performance microscopy gradients – gradients for use in a transverse $\boldsymbol{B}_0$ [41,42]. Even though electromagnets are not used at high fields and transverse access is inconvenient in a supercon, the quadrupolar windings commonly used in atomic beam confinement are sometimes chosen for PFG applications. They permit much higher efficiencies and linearity on two axes (Y and Z, where X is aligned with the coil-form cylinder axis) with respect to $\boldsymbol{B}_Z$ than can be obtained by the standard Maxwellian z-gradient – which outperforms conventional transverse gradients by a factor of 1.5 to 2. These coils owe their improved performance to their ability to produce a pure quadrupolar field throughout almost all of their enclosed volume, while other gradient coils produce substantial higher-order components.

Table 60.1. Doty 3-axes high-field gradient sets (low-impedance option).

Parameter[1]	**Units**[*]	**Model 20-42T**	**Model 24-40**	**Model 50-72S**	**Model 50-72W**	**Model 66-98T**	**Model 85-120W**
Continuous gradient[2], G_C	**mT/m**	2500	340	140	260	140	180
Pulse gradient	**G/cm**	**1500**	**340**	**100**	**90**	**100**	**60**
Pulse duty cycle	%	2	1	2	8	2	9
Rise time[3] **to** G_C	**μs**	12	6	8	20	12	55
Cooling method		water	air	air	water	air	water
Alumina ceramic coil form		yes	yes	yes	yes	yes	yes
Ring down time[4]	**μs**	15	10	15	15	25	40
Gradient null point, $\pm z_0$	**mm**	18	14	25	37	48	52
4% inhomo cylin. Dia., d_1	**mm**	16	15	32	32	46	64
10% inhomo cylin. Dia., d_2	**mm**	18	21	38	38	56	75
10% inhomo cylin., lgh[5]	**mm**	25	20	36	50	50	65
Clear I.D., d_F	**mm**	18.0	22.0	47.0	47.0	66.0	84.6
Cu RF shield dia, d_R	**mm**	20.0	24.0	50.0	50.0	70.0	84.6
Outside dia, d_0	**mm**	42.0	39.7	72.6	72.6	98.0	119.5
Coil half-length, h_0	**mm**	28	24	55	85	85	120
Max L	μH	70	21	35	42	65	130
Max R_E	**Ω**	0.8	0.8	0.6	0.6	0.7	0.6
Grad. Gain, α	**mT/Am**	125	38	8.5	7.5	7.5	4.1
Slew ($\alpha V/L$) at 1 V	**T/m/s**	1800	2000	250	180	110	32
I_{RMS} (single axis)	**A**	20	9	16.5	35	19	45
LF Efficiency, η_L	%	45	5.3	3.8	4.1	11.2	12.2
EPI Acoustic Noise[6]	**dBa**	–	65	70	70	75	75
Nerve stimulation: $\boldsymbol{B}_{max}/\boldsymbol{B}_G$		–	1.3	1.3	1.5	1.3	1.4
Shielding error[7] at 1.5 d_0	%	0.8	0.4	0.5	0.6	0.6	0.6
Total mass	**kg**	0.2	0.2	1.0	1.5	2.5	5.0

(Notes to Table 60.1 see page 672)

Notes to Table 60.1:

1. Performance is indicated with a Techron model 7780 amplifier: 180 A_P; 140 V_P; 100 dB *S/N*; DC-30 kHz power bandwidth. Data for models with T suffix (Transverse B_0) are given for the two strong axes. For the other (standard supercon) models, data are given for the two transverse axes, and performance of the z gradient is considerably better.
2. Continuous rating (100% duty cycle) is indicated for a single axis. For the magic-angle gradient ($X + Y + Z$), the resultant gradient (1.7 G_C) is rated at 50% duty cycle.
3. Rise time, with leads, 5% to 95%, for at least two axes.
4. Ring down, approx. time from 5% to 0.2% with optimized ECC and rf shield.
5. RMS gradient inhomogeneity, excluding 10% chamfer on edges of sample cylinder.
6. Noise, approx. A-weighted; 128 × 128 EPI scan, 30 G/cm read, at 7 T.
7. Shielding error is the relative 1st-order residual gradients from eddies in a cryostat radiation shield 1.4 times the outside diameter of the gradient set.

Table 60.1 includes several of these coils denoted with the suffix T, for Transverse geometry. The data listed for these coils are for the two high-performance axes. The third axis is obtained from a conventional transverse coil design, and its performance is less by at least a factor of 2.

60.6 Conclusion

The switching efficiency is one of the more important figures of merit for high-performance MRI in large samples at high fields because gradient amplifier cost is proportional to $i_P V_P$. High DC efficiency, low current concentration ratios, and high cooling effectiveness are more important in microscopy because of their relationship to maximum continuous and pulsed gradient ratings. The location of the nearest gradient null point is often more important than linearity, as standard methods of specifying the latter have not been agreed upon and distortion correction methods are becoming more successful. Effective RF shielding must be included in the gradient design, and its RF loss is often critical in microscopy but rarely adequately addressed. Achieving low acoustic efficiency and high shielding factor are also extremely important because of their relationship to recovery time, image artifacts, and reliability. Noise, drift, and output impedance in constant-current mode are critical amplifier specifications for microscopy. Perhaps other manufacturers will follow by providing more detailed and well-defined gradient coil specifications to better enable researchers to plan experiments.

References

1. P. Mansfield and B. Chapman, *J. Magn. Reson.* **66** (1986) 573–576.
2. J. Schenck, M. Hussain, and W. Edelstein, *U.S. Pat.* 4,646,024 (1987) GE.
3. F. D. Doty and J. Wilcher, *U.S. Pat.* 5,554,929 (1996) Doty Scientific.
4. D. C. Alsop, T. J. Connick, *Magn. Reson. Med.* **35** (1996) 875–886.
5. W. H. Muller, *U.S. Pat.* 5,406,205 (1995) Bruker.
6. R. Turner, *J. Phys. D: Appl. Phys.* **19** (1986) 151.
7. Y. P. Du and D. L. Parker, *Magn. Reson. Imag.* **14**(2) (1996) 201–207.
8. S. Crozier and D. M. Doddrell, *J. Magn. Reson. A* **103**(3) (1993) 354–357.
9. P. Roemer, *U.S. Pat.* 4,926,125 (1990) GE.
10. P. S. Morgan, R. W. Bowtell, and B. S. Worthington, *Proc. 5th ISMRM*, Vancouver, 1997.
11. N. Gai and L. Axel, *Magn. Reson. Med.* **37** (1997) 275–284.
12. J. J. Van Vaals and A. H. Bergman, *J. Magn. Reson.* **90** (1990) 52–70.
13. D. Barache, J-P. Antoine, J-M. Dereppe, *J. Magn. Reson.* **128** (1997) 30–41.
14. P. B. Roemer and J. S. Hickey, *U.S. Pat.* 4,737,716 (1988) GE.
15. P. Mansfield, B. L. W. Chapman, R. Turner, and R. M. Bowley, *U.S. Pat.* 4,978,920 (1990) N.R.D.C., London.
16. A. M. Abduljalil, A. H. Aletras, and P-M. L. Robitaille, *Magn. Reson. Med.* **31**(4) (1994) 450–3.
17. M. A. Morich, J. L. Patrick and G. D. DeMeester, *U.S. Pat.* 5,424,643 (1995) Picker.
18. Q. Liu, D. G. Hughes, P. S. Allen, *J. Magn. Reson. B* **108** (1995) 205–212.
19. R. J. Ordidge and I. D. Cresshull, *J. Magn. Reson.* **69** (1986) 151–155.
20. P. B. Roemer and W. A. Edelstein, *U.S. Pat.* 4,871,969 (1989) GE.
21. R. Rzedzian and C. Martin, *U.S. Pat.* 5,243,286 (1993) Advanced NMR, Mass.
22. M. H. Buonocore and L. Gao, *Magn. Reson. Med.* **37** (1997) 591–599.
23. G. Pausch, *U.S. Pat.* 5,309,107 (1994) Siemens.
24. M. A. Morich, L. Petropoulos, D. A. Lampman, *U.S. Pat.* 5,485,087 (1996) Picker.
25. R. Hurwitz, S. R. Lane, R. A. Bell, M. N. Brant-Zawadzki, *Radiology* **173** (1989) 545–548.
26. S. A. Counter, A. Olofsson, H. F. Grahn, E. Borg, *J. Magn. Reson. Imag.* **7** (1997) 606–611.
27. G. Miyajima and Y. Igarashi, *U.S. Pat.* 5,256,969 (1993).
28. D. Lehme el al, *U.S. Pat.* 5,235,283 (1993) Siemens.
29. B. Chapman and P. Mansfield, *J. Magn. Reson. B* **107** (1995) 151–157.
30. R. Bowtell and P. Mansfield, *Magn. Reson. Med.* **34** (1995) 494–97.
31. M. J. E. Golay and N. J. Rumson, *U. S. Pat.* 3,569,823 (1971).

32. G. Frese and E. Stetter, *U.S. Pat.* 5,198,769, (1993) Siemens, Munich.

33. W. W. Brey, T. H. Mareci, and J. Dougherty, *J. Magn. Reson. B* **112** (1996) 124–130.

34. L. E. Kinsler, A. R. Frey, *Fundamentals of Acoustics*, 2nd ed., Wiley, NY (1962)

35. P. R. Harvey and P. Mansfield, *Magn. Reson. Med.* **32** (1994) 236–41.

36. R. Muthupillai, P. Rossman, D. Lomas, J. Greenleaf, S. Riederer, R. L. Ehman, *Magn. Reson. Med.* **36** (1996) 266–274.

37. W. F. Wirth and T. G. McFarland, *U.S. Pat.* 5,451,878 (1995) GE.

38. F. D. Doty, G. Entzminger, and A. Yang, *Concepts in NMR* **10** (1998) 133–156.

39. B. H. Suits and D. E. Wilken, *J. Phys. E.* **22** (1989) 565–573.

40. E. C. Wong, A. Jesmanowicz, and J. S. Hyde, *Magn. Reson. Med.* **21** (1991) 39–48.

41. R. A. Beth, *U.S. Pat.* 3,466,499 (1969).

42. R. Bowtell and P. Mansfield, *Meas. Sci. Technol.* **1** (1990) 431–439.